Koskela, Sanna; Turunen, Tuomas; Ala-Laurila, Petri

Mice Reach Higher Visual Sensitivity at Night by Using a More Efficient Behavioral Strategy

Published in:
Current Biology

DOI:
10.1016/j.cub.2019.11.021

Published: 06/01/2020

Document Version
Publisher's PDF, also known as Version of record

Article

Current Biology

Mice Reach Higher Visual Sensitivity at Night by Using a More Efficient Behavioral Strategy

Graphical Abstract

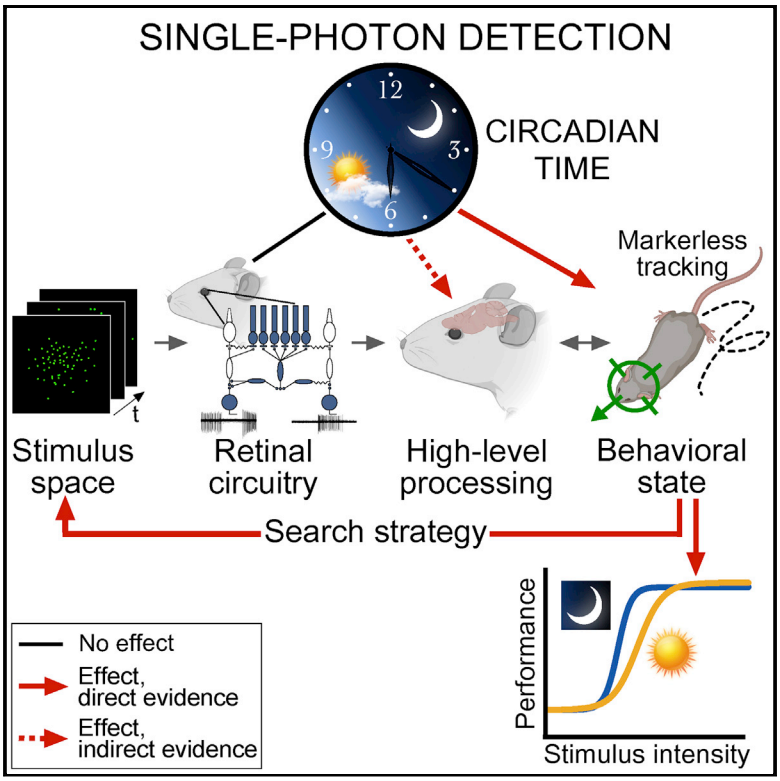

Authors

Sanna Koskela, Tuomas Turunen, Petri Ala-Laurila

Correspondence

petri.ala-laurila@helsinki.fi

In Brief

Koskela et al. unravel the impact of diurnal rhythm on single-photon detection from retinal circuits to behavior. Surprisingly, mice reach higher sensitivity at night even if the relevant retinal ganglion cells do not show diurnal differences. Mice employ a better search strategy associated with more efficient higher-order processing at night.

Highlights

- Diurnal effects on visual sensitivity were studied from the retina to behavior
- Visually guided behavior of mice reaches the highest sensitivity at night
- The sensitivity limit of retinal ganglion cells does not show diurnal differences
- Mice use a better search strategy for visual cues at night

Koskela et al., 2020, Current Biology *30*, 42–53
January 6, 2020
https://doi.org/10.1016/j.cub.2019.11.021

CellPress

CellPress

Current Biology
Article

Mice Reach Higher Visual Sensitivity at Night by Using a More Efficient Behavioral Strategy

Sanna Koskela,[1] Tuomas Turunen,[1,2] and Petri Ala-Laurila[1,2,3,*]
[1]Faculty of Biological and Environmental Sciences, Molecular and Integrative Biosciences Research Programme, University of Helsinki, 00790 Helsinki, Finland
[2]Department of Neuroscience and Biomedical Engineering, Aalto University School of Science, 02150 Espoo, Finland
[3]Lead Contact
*Correspondence: petri.ala-laurila@helsinki.fi
https://doi.org/10.1016/j.cub.2019.11.021

SUMMARY

Circadian clocks predictively adjust the physiology of organisms to the day/night cycle. The retina has its own clock, and many diurnal changes in its physiology have been reported. However, their implications for retinal functions and visually guided behavior are largely unresolved. Here, we study the impact of diurnal rhythm on the sensitivity limit of mouse vision. A simple photon detection task allowed us to link well-defined retinal output signals directly to visually guided behavior. We show that visually guided behavior at its sensitivity limit is strongly under diurnal control, reaching the highest sensitivity and stability at night. The diurnal differences in visual sensitivity did not arise in the retina, as assessed by spike recordings from the most sensitive retinal ganglion cell types: ON sustained, OFF sustained, and OFF transient alpha ganglion cells. Instead, we found that mice, as nocturnal animals, use a more efficient search strategy for visual cues at night. Intriguingly, they can switch to the more efficient night strategy even at their subjective day after first having performed the task at night. Our results exemplify that the shape of visual psychometric functions depends robustly on the diurnal state of the animal, its search strategy, and even its diurnal history of performing the task. The results highlight the impact of the day/night cycle on high-level sensory processing, demonstrating a direct diurnal impact on the behavioral strategy of the animal.

INTRODUCTION

Vast differences in light intensity between day and night set strict functional demands on the reliability and adaptability of visual functions. Many retinal mechanisms operating at different circuit locations and on multiple timescales contribute to direct stimulus-dependent visual adaptations [1–4]; for reviews, see [5–7]. Humans, like other mammals, have an intrinsic clock in the suprachiasmatic nucleus (SCN) that is synchronized by the intrinsically photosensitive retinal ganglion cells (ipRGCs) driving non-image-forming visual functions like the pupillary light reflex [8–13], for reviews, see [14, 15]. However, it has remained mostly unknown to what extent the diurnal rhythm has direct functional impact on retinal computations and retinal output signals. Can diurnal rhythm contribute to the adaptive processes of image-forming vision by anticipating the different functional needs of vision between the day and the night?

A rich set of diurnal changes in retinal biochemistry and physiology has been reported. The concentration and expression levels of neurotransmitters and many key signaling molecules in the retina show circadian and/or diurnal changes, including the neuromodulators dopamine [16, 17] and melatonin [18], melatonin receptors [19], as well as melanopsin in ipRGCs [20–22]. The internal messenger cAMP shows diurnal changes in photoreceptors [23, 24] that have been suggested to cause different signal and noise distributions in rods [25]. Even the expression of different types of visual pigment molecules in photoreceptors in some species has been shown to be dependent on the time of the day/night cycle [26, 27]. Furthermore, disk shedding in rods is under diurnal control [28], and a recent study even reports differences in the rate of the visual cycle between day and night [29]. Retinal signals, as assessed by electroretinogram, show diurnal amplitude variations [30–34], as does electrical coupling between rods and cones [35], rods and rods [36], between AII amacrine cells [37], as well as between RGCs [38]. The intrinsically photosensitive M4 cells of rat (also known as ON sustained alpha RGCs) have higher firing rates in the daytime [39]. Similarly, a recent study relying on recordings from single RGCs in awake mice *in vivo* revealed circadian variation in the firing rates of directionally selective RGCs and some other RGC types over multiple day/night cycles [40]. Finally, differences in the inhibitory signaling of RGCs have been shown to depend on melatonin levels [41]. Despite this extensive circadian modulation at the molecular and cellular levels as well as in retinal circuit connectivity, little is known about the functional implications of these circadian changes on retinal computations and visually guided behavior in rodents.

Human studies have reported diurnal changes at both the photopic and scotopic sensitivity thresholds [42, 43]. Similarly, small diurnal differences in decrement detection thresholds across dim background lights have been reported in mice in a water maze task [44]. It has been commonly hypothesized that these changes in visual sensitivity at the behavioral level relate to physiological changes in the retina [35, 44, 45], but direct experimental evidence is missing.

Here, we have measured the impact of diurnal rhythm on the visual sensitivity of mice, both at the level of the most sensitive retinal ganglion cell types and visually guided behavior. Single-photon detection at the sensitivity limit of vision provides a uniquely simplified framework to study diurnal effects from well-defined, functionally relevant retinal outputs to visually guided behavior. Our recent work relying on this task has shown that behavioral performance of mice can be linked to the spike outputs of ON sustained alpha RGCs [46]. To assess the possible role of melatonin in diurnal changes of visual functions, we performed the same experiments on two mouse strains: CBA/CaJ (hereafter abbreviated CBA) mice that have melatonin [47] and C57BL/6J (hereafter abbreviated C57) mice that do not have a robust melatonin rhythm [48] but still have a diurnal rhythm potentially due to dopamine [17].

RESULTS

Mice Have Higher Behavioral Sensitivity in Light Detection at Night Than at Day

First, we tested the hypothesis that mouse vision is more sensitive during the night than during the day as assessed behaviorally in a dim-light detection task (Figure 1A). CBA and C57 mice were split into two groups (Figure 1B): one group was tested during their subjective day ("day group") and the other group during their subjective night ("night group"). Both groups were acclimated to their respective diurnal rhythms, and the adjustment was confirmed by monitoring running-wheel activity in their housing conditions (STAR Methods). Figures 1C and 1D show the running wheel activity of individual mice in the day group (top panels) and in the night group (bottom panels) for both CBA (Figure 1C) and C57 (Figure 1D) mice. The population average across all mice is shown below each actogram. The running-wheel activity of both mouse strains showed a clear diurnal dependence, with the peak activity appearing soon after light offset.

We measured the pupil sizes of dark-adapted mice corresponding to the times at which behavioral measurements were conducted. This was done to separate potential optical effects from neural effects on visual sensitivity (Figures 1E and 1G) by taking differences in pupil size into account in our conversion of light intensities into photoisomerization rates (Figures 1I–1J, see STAR Methods). There was a slight but significant increase (7%–9%) in the pupil size during the subjective night, both in C57 ($p < 0.0001$, paired samples t test) and in CBA mice ($p < 0.02$). These changes cannot impact behavioral sensitivity in our measurements, where they are already accounted for in photoisomerization calculations. However, they could still be interesting indicators of the internal state of the animals (e.g., arousal, see Discussion).

Our main interest here was visually guided behavior as assessed in a dim-light detection task in a water maze in the dark. All mice had been trained to associate an escape ramp from the water with a light stimulus during a training period preceding the experiments where different stimulus intensities were used (Figures 1A, 1F, and 1H). The training ended when the performance of both the day and the night groups for an easily detectable bright stimulus light stabilized at a level of $\geq$80% correct choices, which occurred after ~12 days of training in both the day and the night groups. Figures 1I and 1J show the psychometric functions for light detection for the night groups (blue) and the day groups (gold). All groups were dark-adapted for at least 2 h prior to the experiments (Figure 1B). The times of the day when the mouse groups were tested in the behavioral experiments are indicated as bars on top of the light/dark cycle schematics in Figure 1B. Figures 1I and 1J show a robust difference in visual sensitivity between the day and the night groups: mice in the night group were more likely to find the stimulus corridor in the maze as the first choice over a large range of the dimmest stimulus intensities. The shape of the psychometric functions between the day and the night groups differed significantly: the slope parameter n for both CBA and C57 being ~2 times greater for the night group (see Equation 1 in Figure 1 legend). The intensity needed for half-maximal performance (fit parameter K_m) was significantly lower at night compared to that at day: 13-fold in CBA and 7-fold in C57. By contrast, the intensity at which the psychometric functions started to deviate from the chance level (~0.01 visual pigment isomerizations per rod per second, R*/rod/s) was similar for both the day and the night groups, consistent with the idea of a shared ultimate neural constraint (see Discussion).

We also tested CBA mice at the time of night when melatonin levels are reported to be the highest [49] (indicated by a red bar in Figure 1B). Performance at this testing time was similar to that at the other testing time during the subjective night (cf. red and blue traces in Figure 1I). Moreover, CBA and C57 mice showed very similar performance at their subjective night: the light intensity needed for half-maximal performance was ~0.02 R*/rod/s for both strains. Thus, the diurnal differences in behavior were not dependent on the melatonin proficiency or deficiency of mouse strains nor on the prevailing melatonin level in CBA. The performance levels at subjective night were stable and consistent across the two mouse lines.

The Most Sensitive RGCs Do Not Show Strong Diurnal Changes in Their Threshold Sensitivity

We wanted to test whether the diurnal changes in visually guided behavior arise already in the retinal signal processing. In general, linking retinal function to behavior is particularly difficult since the functional connection between the spike codes originating from the populations of ~40 distinct RGC types [50–52] and behavior has not been established. Vision at its sensitivity limit provides a unique opportunity to crucially simplify this challenge, as visual information arising from sparse photons is encoded only by a limited number of RGC types. In recent study, we targeted all unidentified RGC types in complete RGC mosaics across ~200 RGCs and showed that ON sustained (ON-S), OFF sustained (OFF-S), and OFF transient (OFF-T) alpha RGCs constituted the most sensitive RGC types of the mouse retina [46]. Furthermore, we showed by relying on a transgenic mouse line with a sensitivity shift in the ON pathway that behavioral light detection at the sensitivity limit is driven only by the ON-S RGCs. Now we utilized this single-photon detection paradigm to study the retinal contribution to the observed diurnal changes in behavior.

Here, we measured the spike outputs of all of these most sensitive mouse RGC types—ON-S, OFF-S, OFF-T alpha RGCs—*ex vivo* in dark-adapted flat-mounted mouse retinas with the

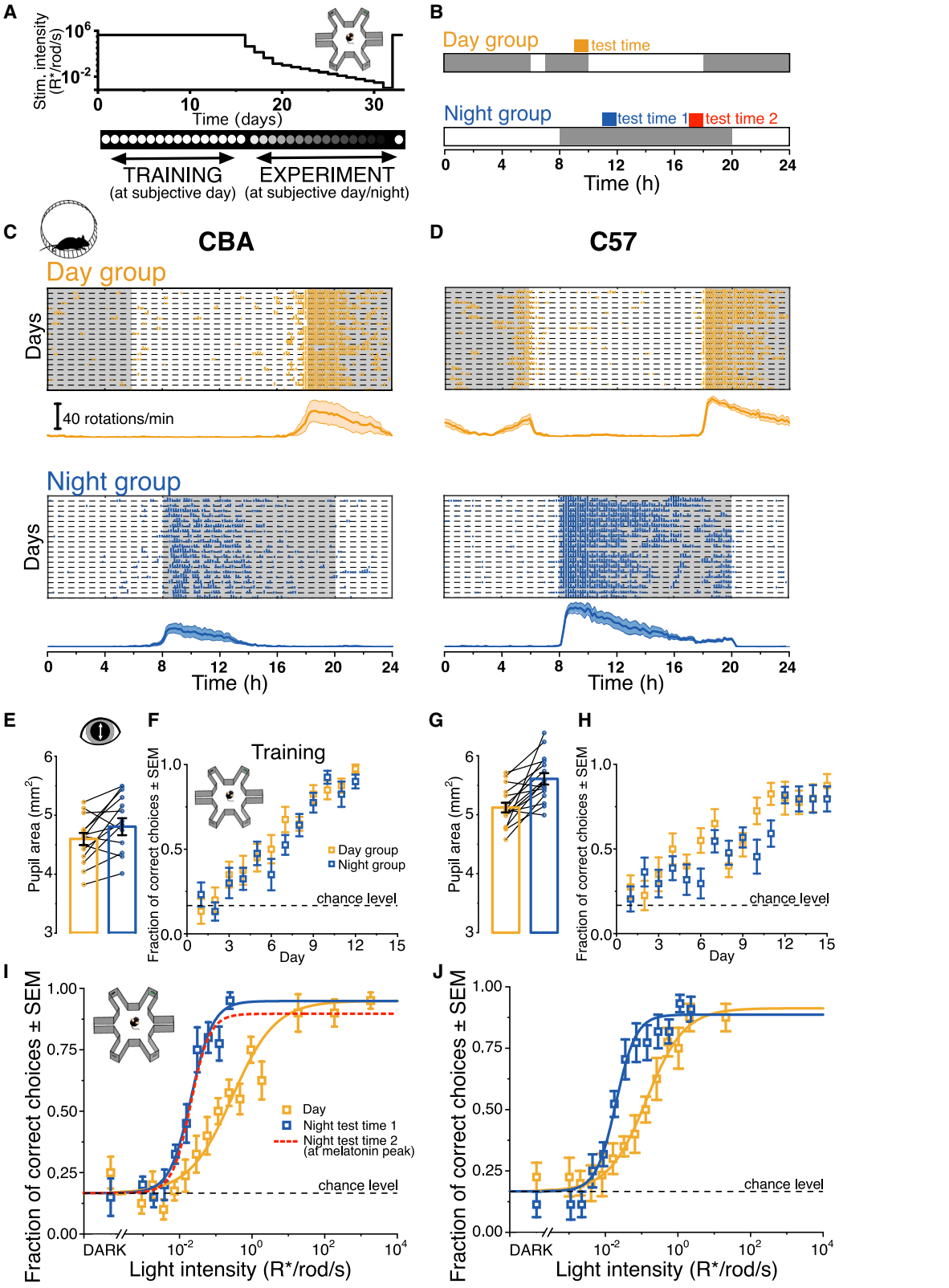

(legend on next page)

particular interest in the ON-S RGCs. We recorded the responses of alpha RGCs to sequences of flashes at intensities close to the detection threshold at times of the subjective day and the subjective night corresponding to the behavioral testing times. Figure 2 shows example spike rasters of such measurements at four increasing flash intensities for CBA ON-S (Figure 2A), OFF-S (Figure 2B), and OFF-T RGCs (Figure 2C) tested at subjective day (gold) and subjective night (blue). Figures 2D–2F show the mean firing rates for each of the stimulus intensities. These flash intensities (from the lowest to the highest intensity) elicit only ~10–200 visual pigment isomerizations (R*) in the entire receptive field of the RGC assuming a collecting area of 10,000 rods [53]. We used two-alternative forced choice (2AFC) ideal observer analysis to define the sensitivity limit of RGCs based on these spike responses as previously described ([54]; STAR Methods). Discrimination was based on computing the correlation between the mean response and each epoch during the intervals before and after the flash. The task was to determine which of the two intervals was more likely to contain a response to the flash. Figures 2G–2I show 2AFC results calculated from the same example recordings as shown in Figures 2A–2C. We defined the RGC detection threshold as the light intensity giving a 75% fraction of correct choices in this task. Figure 2J shows the population data on detection thresholds. OFF-S and OFF-T RGCs were slightly more sensitive (<3-fold; see Table S1) than ON-S RGCs for both mouse lines, consistent with previous literature both in mouse [55] and in primate [54]. Most importantly, no significant day-night differences in the detection thresholds of the ON-RGCs between the day and the night were seen in either the CBA or the C57 mouse strains (CBA: p = 0.88, C57: p = 0.94, two-independent-samples t test). Likewise, the day-night differences in the detection thresholds of OFF-S and OFF-T RGCs were not significant (OFF-S CBA: p = 0.14, C57: p = 0.78; OFF-T CBA: p = 0.08, C57: p = 0.19). We also measured the sensitivity of a subset of CBA ON-S RGCs to longer 500-ms light steps in addition to flashes. The sensitivity to light steps did not differ between the day and night (p = 0.95, two-independent-samples t test, Table S1). The lack of diurnal differences in ON-S RGCs is the most important for behavioral sensitivity comparisons, since our recent work relying on a transgenic mouse strain shows that visually guided behavior at the sensitivity limit of vision correlates closely with the performance of ON-S alpha but not OFF-S RGCs [46].

To assess whether other aspects of spike responses could indicate day-night differences, we also compared the spontaneous firing rates and flash sensitivities (spikes elicited per photoisomerization) of RGCs between the day and night groups. The spontaneous firing rates of ON-S and OFF-S RGCs differed significantly from each other for both CBA and C57 mice consistent with previous studies (for mouse, see [55]; for primate ON and OFF parasol cells, i.e., the closest homologs of mouse alpha RGCs, see [54]). Comparing strains, CBA ON-S RGCs had a lower tonic firing rate than C57 ON-S RGCs (mean firing rate ±SEM, Hz): 2.1 ± 0.5 Hz (CBA, ON-S, n = 47) versus 12 ± 1.9 Hz (C57, ON-S, n = 40), while both the CBA OFF-S and OFF-T RGCs had a higher tonic firing rate than C57 OFF RGCs: 74 ± 1.9 Hz (CBA, OFF-S, n = 61) versus 62 ± 2.4 Hz (C57, OFF-S, n = 35); 33 ± 1.4 Hz (CBA, OFF-T,

Figure 1. Mice Reach Higher Visual Sensitivity in a Dim-Light Detection Task in a Water Maze during Their Subjective Night Compared with Their Subjective Day

(A) Experimental protocol consisting of a training period (12–15 days; done at subjective day for all mice) with a constant bright stimulus light and followed by an experimental period (10–16 days; done at subjective night for the night group and at subjective day for the day group). During the experiment, the light intensity was made dimmer in each testing day. At the end of the experimental series, the mice were re-tested at a high intensity to ensure that no significant changes had happened in their overall ability to perform the task.

(B) Light cycles (12 h/12 h light/dark) for the day group (above) and the night group (below): light period (white), dark period (gray). Behavioral tests were carried out on dark-adapted mice in the time windows indicated by bars above the light cycles: day group = gold bar (tested at 3 h from the light onset); night group = blue bar (tested at 3 h from the light offset, test time 1), The day group was dark-adapted for 2 h during their light period in behavioral experiments (gray bar). The "test time 2" above the night group (red bar) marks the time when melatonin levels are estimated to be highest (9 h after light offset [49]), and the CBA night group was additionally tested at this time.

(C) Running-wheel actograms for CBA mice housed under the light cycles shown in (B) plotted on a 24-h timescale: day group above (gold), night group below (blue); light period (white), dark period (gray). Actograms exemplify the activity profile of an individual mouse as a function of time on 20 successive days (in 10-min time bins; in 15 quantiles with the first being 1–55 revolutions, the second 56–110, and so on). Bottom: the mean activity profiles (the width of each trace indicates mean ± SEM); day group n = 4 mice; night group n = 6. The scale bar is the same for all mean activity profiles.

(D) The same as (C) but showing results for C57 mice. Mean activity profiles for day and night groups: n = 8.

(E) The pupil areas of CBA mice measured at behavioral testing times are shown in bar graphs (mean ± SEM, mm^2): 4.6 ± 0.1 (day, gold); 4.9 ± 0.1 (night, blue). Symbols connected by lines are from the same mouse (n = 14).

(F) Training data of the day (gold, n = 10) and the night (blue, n = 10) group of CBA mice in a behavioral light detection task in a water maze using a single easily detectable stimulus light intensity. The dashed line indicates the chance level of 0.17 (= 1/6). The fraction of correct choices is plotted against the training day: mean across animals ±SEM.

(G) The same as (E) but for C57 mice (n = 16, mean ± SEM, mm^2): 5.1 ± 0.08 (day, gold); 5.6 ± 0.1 (night, blue).

(H) The same as (F) but for C57 mice (day n = 10, night n = 11).

(I) Behavioral visual sensitivity of dark-adapted CBA mice measured in a dim-light detection task in a six-armed water maze tested at day (see testing times in (B) and at night: day group (gold symbols, n = 10), night group (blue symbols, n = 10). The fraction of correct choices is plotted against the light intensity (rate of photoisomerizations, R*/rod/s). Each data point is a mean across animals at that intensity ±SEM. Smooth fits are from Equation 1, STAR Methods: $F = 0.17 + F_{max} \cdot I^n/(I^n + K_m^n)$ with parameters: $K_m = 0.29$, $F_{max} = 0.78$, $n = 0.73$ (day, gold, coefficient of determination $r^2 = 0.97$) and $K_m = 0.02$, $F_{max} = 0.78$, $n = 1.45$ (night, blue, $r^2 = 0.99$). Red dashed line shows the smooth fit to dataset measured at the time corresponding to the melatonin peak (data omitted for clarity, n = 9), with parameters $K_m = 0.02$, $F_{max} = 0.73$, $n = 1.68$.

(J) The same as (I) but showing results on C57 mice (day: n = 10, night: n = 11). Smooth fit from Equation 1 with parameters: $K_m = 0.14$, $F_{max} = 0.75$, $n = 0.83$ (day, gold, $r^2 = 0.98$); $K_m = 0.02$, $F_{max} = 0.72$, $n = 1.57$ (night, blue, $r^2 = 0.98$). The slope (n) and half-saturating intensity (K_m) parameters between the day and the night groups differed significantly for both CBA and C57 as assessed by the posterior probability of a logistic regression fit (see STAR Methods).

See also Figure S1.

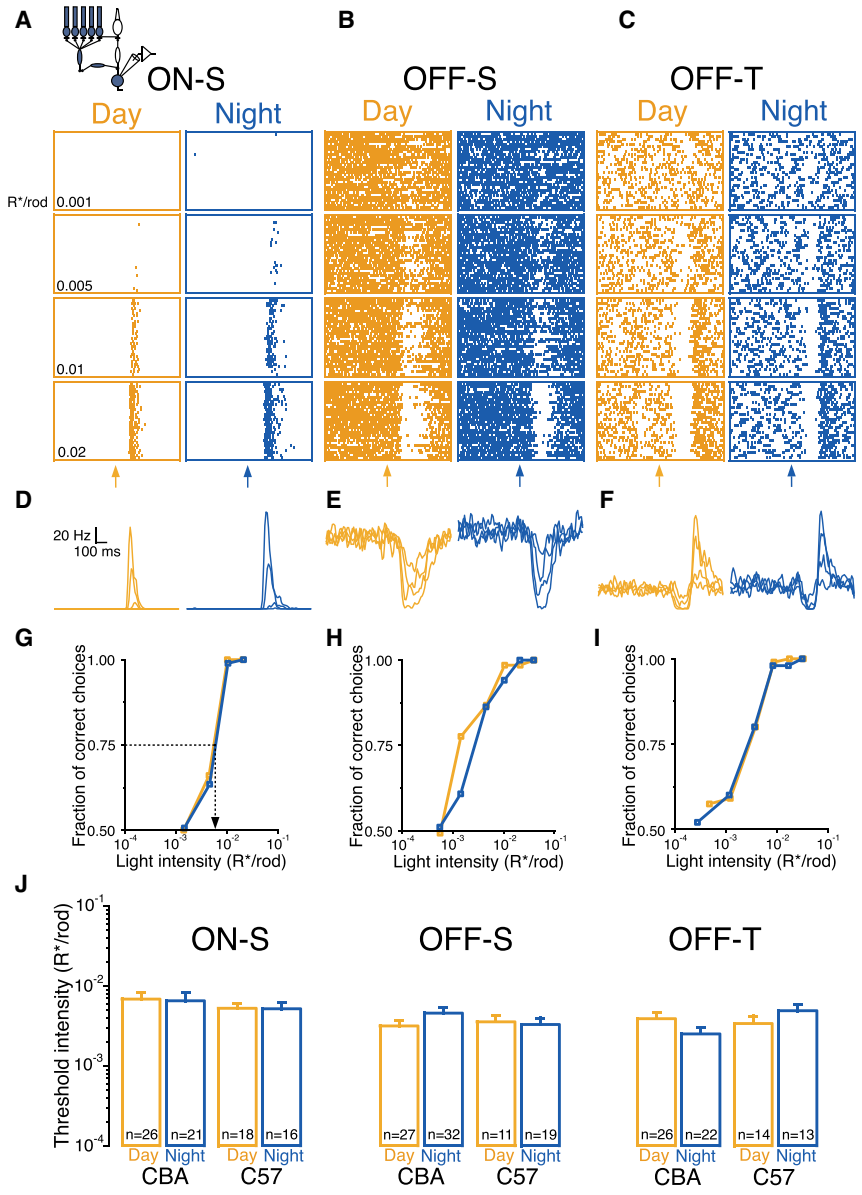

Figure 2. The Sensitivity Limits of Retinal ON-S, OFF-S, and OFF-T alpha RGCs Do Not Show Strong Diurnal Variation

(A) Spike rasters showing responses (n = 30) of a CBA ON-S RGC to a family of 20-ms flashes (delivered at the time of the arrow) of fixed intensities (lower left corner in each box, in R*/rod/flash) measured at subjective day (gold) and subjective night (blue). These are two different example cells from two different retinas.

(B and C) Single OFF-S (B) and OFF-T (C) cell spike responses from a CBA mouse measured at subjective day (gold) and subjective night (blue) to the same flash intensities as in (A).

(D) ON-S cell mean firing rates (PSTH; 10-ms time bin, n = 50) for the same cells and flash intensities as in (A).

(E and F) OFF-S (E) and OFF-T (F) cell mean firing rates for the same cells and flash intensities as in (B) (n = 50).

(G–I) Two-alternative forced choice task for the same ON-S (G), OFF-S (H), and OFF-T (I) RGCs as in (A)–(C).

(J) Threshold intensities for a population of ON-S, OFF-S, and OFF-T RGCs at day and at night from CBA and C57 mouse strains. Bar graphs show mean + SEM. See also Table S1.

n = 50) versus 25 ± 1.5 Hz (C57, OFF-T, n = 29). Consistent with the mean rates, the variances of the spontaneous firing rates in ON-S RGCs were significantly lower in CBA than in C57 mice (mean variance ±SEM, Hz^2): 10 ± 2.3 (CBA, n = 47) versus 81 ± 16 (C57, n = 40). However, no significant day-night differences were found in the intrinsic firing rates (see Table S1). These findings exclude the possibility that differences in retinal noise as measured in the key outputs would underlie the differences in the shapes of psychometric functions between night and day. Furthermore, neither the maximal spike count per photoisomerization (peak flash sensitivity or signal gain, Table S1) nor the integration time differed significantly between the day and the night at the level of RGCs. Neither did we find any significant day-night differences in other spike response metrics that we tested, with the variance of the OFF-T firing rate as the sole exception (Table S1).

Mice Use a More Efficient Search Strategy for Visual Cues at Night

What then underlies the diurnal change in behaviorally measured visual sensitivity? Since diurnal changes in the retinal output signals do not explain the observed behavioral effects, these differences must arise downstream of the retina in the efficiency of sensory processing and/or from differences in the behavioral strategy used to sample visual space. To investigate this further, we took two primary approaches. First, we wanted to test whether the differences in behaviorally measured psychometric sensitivity curves are tightly associated with the testing time of the day/night cycle. Second, we wanted to test whether these sensitivity differences can be associated with the behavioral strategy of mice as quantified by several trackable features of mouse behavior.

We first tested whether the behaviorally measured differences in visual sensitivity between the day and night groups are reversible. In other words, if the measured differences in performance are linked only to the testing time during the day/night cycle, the effects should reverse when the day group is tested at night and vice versa (see Figure 3A). The dashed horizontal lines in Figure 3B show behavioral sensitivity measured at the stimulus intensity where the day/night difference was greatest in the original measurements (red arrow in Figure 3B). The performance of the day group after the swap (i.e., now tested at night; green symbol following axis break in Figure 3B) reached the performance level observed for the original night group (blue dashed line) in line with the idea that the performance level correlates

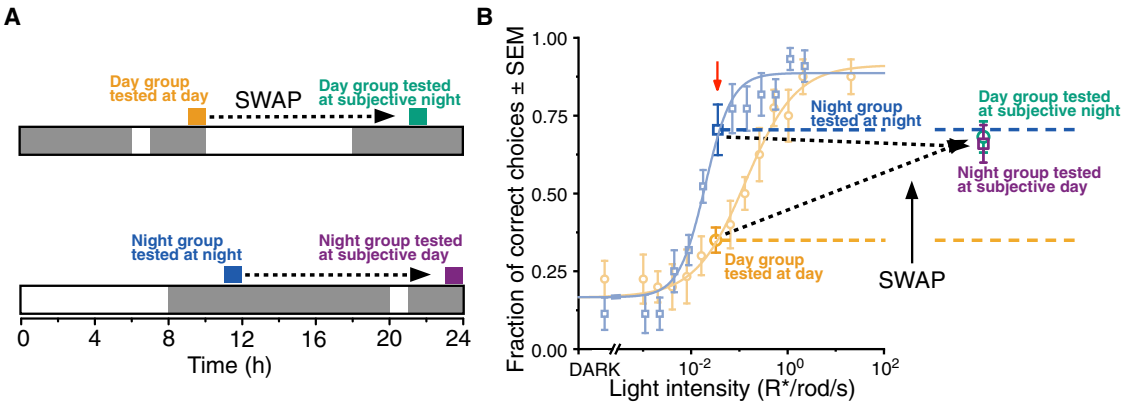

Figure 3. The Mice Are Able to Perform Equally Well in Their Subjective Day after They Have Performed the Visual Task in Their Subjective Night

(A) Scheme of the "swap" experiments, where the testing time of mice was swapped for both day and night mouse groups so that the day group was tested during their subjective night (green bar) and the night group was tested during their subjective day (purple bar). Mice were kept in two different 12 h/12 h light/dark cycles, plotted on a 24-h timescale: day group above and night group below; light period (white), dark period (gray). The behavioral testing times were changed so that day group (gold bar) was tested at night (green bar; 3 h from light offset) and night group (blue bar) was tested during their day (purple bar; 3 h from light onset). (B) Left: the fraction of correct choices against light intensity is shown for the day and night groups before the swap. This is the same data as in Figure 1J (C57 mouse strain). Right: fraction of correct choices (mean ± SEM) averaged across 3 days (steady-state) following the swap tested with a single intensity (red arrow, 0.03 R*/rod/s, where the maximal day-night difference was observed before the swap): 131 trials (night group tested at subjective day, purple), 118 trials (day group tested at subjective night, green). Dashed lines show the performance levels of day group (gold) and night group (blue) before the swap. Square symbols show the mice (n = 11) that were originally tested at their subjective night and now tested at their subjective day after the swap. Circle symbols show the group of mice (n = 10) that were originally tested during their subjective day and now tested at their subjective night after the swap.

with the diurnal phase. Surprisingly, the night group (purple symbol following axis break in Figure 3B) was able to maintain its original high performance level (blue dashed line) after the swap (i.e., now tested at day). These data, together with the RGC data, point toward a neural location other than the retina underlying the behavioral differences and/or a difference in the sampling strategy of visual cues. Such a diurnal history dependence in performance levels would be very unlikely to arise in retinal circuits.

Next, we wanted to test whether the observed differences in behavior originate from how mice sample visual cues (i.e., their behavioral strategy). We used our tracking technology to quantify mouse head and body positions in each video frame and analyzed the mouse behavioral strategy in the center of the maze before the decision to enter a certain corridor (see STAR Methods). This was done in the intensity range corresponding to the greatest day-night difference in the original behavioral dataset (0.03–0.14 R*/rod/s). We used a range of behavioral features (12 in total) listed in Table 1. Some features related to the body position of mice have also been used in earlier literature [56] in the context of other visual tasks at higher light levels. Several other features related to the head orientation of mice are unique for this study relying on our novel tracking technology of the head position and orientation of mice in darkness. The behavioral features differed significantly between the original subjective day and subjective night groups as shown in Table 1, in line with the idea that there is a clear difference in behavioral patterns between the day and night mouse groups ($p < 0.03$ for all features, Mann-Whitney U test for continuous features and a permutation test for discretized features, see Table 1). Figure 4 exemplifies two key features for the day and night groups: one related to body position (the distance of mice from the maze center during swimming trials) and one related to head orientation (the total time that the stimulus is in the visual field while the mouse is making the selection between different channels in the center of the maze). Figures 4A–4C show location heatmaps and location histograms of mice relative to the maze center during the swimming trials for the original day and the original night groups. Indeed, mice in the night group stayed significantly longer on average in the center of the maze collecting information of the correct stimulus corridor (see Table 1: "Swimming distance from center": $p = 0.004$, Mann-Whitney U test). Similarly, Figure 4E shows that the total time that the mice sampled data from the stimulus channel was significantly longer for the night group ($p < 2 \cdot 10^{-8}$, Mann-Whitney U test; see Table 1 "Time stimulus in view"). Furthermore, in the day group, more mice (~18%) made their decision without sampling any information at all from the stimulus channel, whereas, for the night group, the corresponding fraction was <10% (bars corresponding to $\Delta t = 0$ in Figure 4E inset). In summary, both of these features can directly affect behavioral performance: the longer the mice stay at the center of the maze seeking the stimulus and the longer the stimulus falls in their visual field, the more confidently they can make a correct first choice.

We wanted to understand more broadly whether the feature space studied and showing differences between the day and night groups also correlates with the actual behavioral performance as quantified by fraction of correct choices in the 6AFC task. Since behavioral performance becomes similar for both day and night groups after the swap, the differences in the behavioral features between the groups should also disappear if indeed the behavioral pattern captured by these features is associated with the performance in the 6AFC task. Indeed, we observed that 10 out of 12 features that differed significantly

Table 1. Behavioral Features from the Automatic Video Tracking System Compared between Day and Night

	Before Swap			After Swap		
Features	Day	Night	p Value	Night	Day	p Value
Body Position						
Swimming distance (mm)	190	218	0.024*	182	181	0.802
Swimming distance from center (mm)	56	46	0.004*	57	52	0.082
Swimming speed (mm/s)	145	136	0.002*	150	128	4.9×10^{-5}*
Swimming time (s)	1.1	1.4	1.5×10^{-4}*	1.1	1.2	0.148
Head Direction						
Angular velocity (deg/s)	101	133	4.8×10^{-4}*	121	107	0.049*
Heading angle (deg)	86	46	3.0×10^{-4}*	49	60	0.576
Meander (deg/mm)	0.7	0.9	0.001*	0.8	0.8	0.538
Number of corridors seen	5.1	5.4	0.013*	5.0	5.0	0.901
Time stimulus in view (s)	0.7	1.0	2.2×10^{-8}*	0.8	0.9	0.186
Times correct corridor comes into view	1.0	1.2	0.005*	1.1	1.2	0.068
Times new corridor comes into view	6.0	7.3	2.0×10^{-5}*	6.3	6.5	0.696
Turn angle (deg)	217	271	0.002*	226	209	0.956

"Before swap" indicates the day group tested at day and night group tested at night. "After swap" indicates day group tested at subjective night and night group tested at subjective day. The features are explained below. To exclude the time after the mouse has detected the stimulus and merely swims toward it, the analysis is focused on the early part of the trial corresponding to 50% of the maze area (see STAR Methods). In this constrained area, the analysis starts when the mouse is freed to swim and ends when the mouse exits this central region toward any corridor. The mouse visual field is assumed to be ±100°. The analysis is done on the intensity range of 0.03–0.14 R*/rod/s, where the maximal day/night performance difference was observed (see Figures 1G and 1H). Nonparametric Mann-Whitney U test was used to test the difference in medians between night and day in all of the continuous behavioral features and permutation test [88] with mean as a test statistic in the discretized features (Number of corridors seen, Times correct corridor comes into view, Times new corridor comes in to view). The statistically significant values ($p < 0.05$) are marked with an asterisk. The sample sizes were the following: day group before swap n = 115 trials; night group before swap n = 130 trials; day group after swap n = 118 trials; night group after swap n = 131 trials.

Feature explanations: *swimming distance*: the total path length (mm). *Swimming distance from center*: the median distance of the mouse from the maze center on its swimming path (mm). *Swimming speed*: the median swimming speed of the mouse (mm/s). *Swimming time*: the total swimming time for the mouse to exit the central region (s). *Angular velocity*: the median turning speed of the mouse on its swimming path (degrees/s). Total turning (degrees) divided by the total swimming time (s). *Heading angle*: the median angle between the head-direction of the mouse and the direction of the stimulus relative to the mouse head (degrees). A small heading angle indicates that the mouse has been mainly looking at the stimulus. *Meander (= zigzag)*: the change in the direction of movement of the mouse relative to the distance it moves (degrees/mm). A small value in meander indicates that mouse swam a straight route from start to the target. *Number of corridors seen*: count of how many of the six light-emitting diodes (LEDs) (the stimulus LED is on, the other five LEDs are off) have fallen inside the visual field of the mouse on its swimming path. *Time stimulus in view*: the accumulated time the stimulus stays within the visual field (s). *Times correct corridor comes into view*: the number of times the stimulus LED enters the visual field. The number increases each time when the stimulus appears in the visual field after being absent from the visual field. *Times new corridor comes into view*: the number of times any LED (the stimulus LED or any other LED) falls within the mouse visual field. The number increases when the mouse looks into the same LED multiple times. *Turn angle*: the cumulative change in direction during the swimming path (degrees). A large turn angle indicates circling movements.

before the swap became similar after the swap (see Table 1). Figures 4D and 4F exemplify that both the swimming location relative to the center of the maze and the total time that the stimulus is in the visual field became very similar after the swap ($p = 0.08$, and $p = 0.19$, respectively, Mann-Whitney U test; see Table 1). Similarly, the fraction of mice that do not sample at all from the stimulus before making a choice became similar and much smaller than in the original day group (bars corresponding to $\Delta t = 0$ in Figure 4F, inset). Significant differences only remain for two of the 12 features: angular velocity and swimming speed (see Table 1). Despite these two features, our data are, overall, consistent with the notion that there is a robust difference in behavior as quantified over a wide range of body position and head-orientation-related features between the day and night groups. Furthermore, the results after the swap demonstrate that these features can be qualitatively linked to the performance of the mice in the 6AFC task.

DISCUSSION

We show that psychometric functions in a behavioral photon detection task are under diurnal control and that mice reach higher visual sensitivity at night. This change correlates with a different behavioral repertoire between the subjective day and the subjective night as characterized by multiple behavioral features. Several of these features suggest that mice use a more efficient behavioral strategy for visual cues at their subjective night. Intriguingly, improvements in the search strategy are

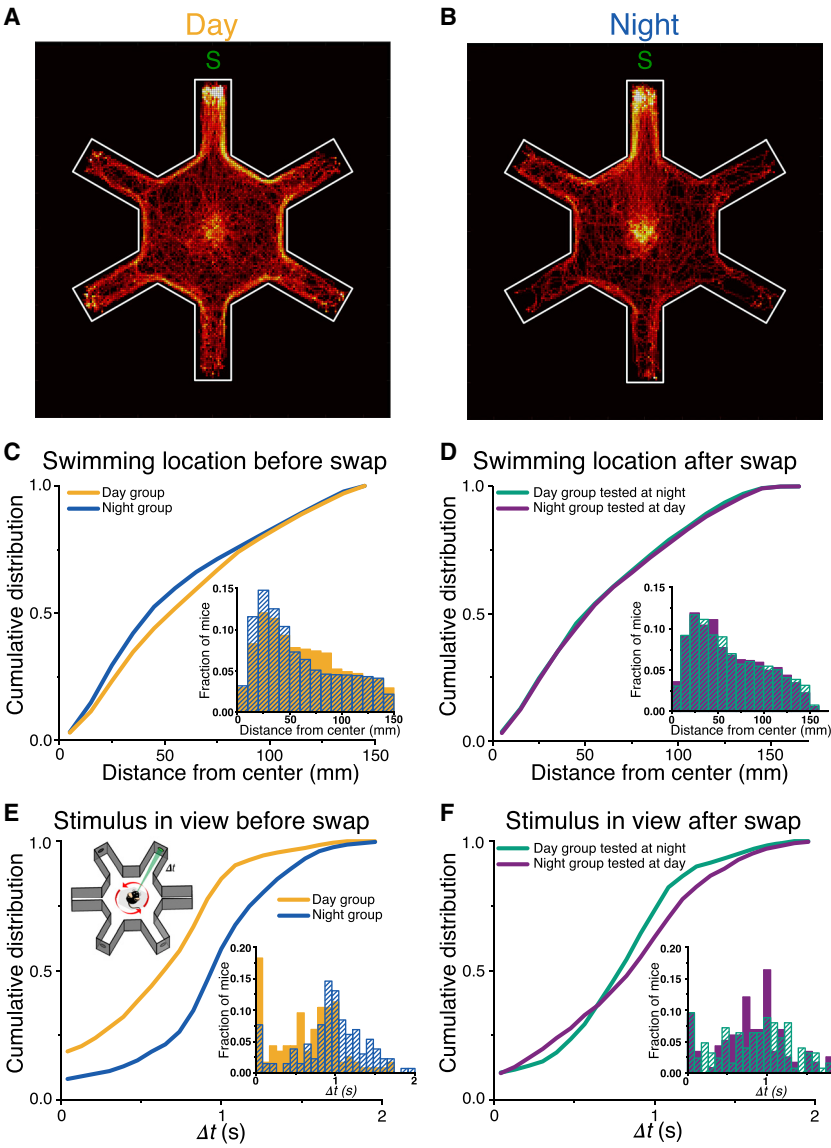

Figure 4. Mice Use a More Efficient Search Strategy for Visual Cues at Night

(A) Tracked population swimming paths of 115 trials of mice (C57) in their day for the intensity range 0.03–0.14 R*/rod/s, where the maximal day/night performance difference was observed (see the psychometric functions, Figures 1I and 1J). The "correct" corridor with the light stimulus is marked with S.

(B) The same as (A) but shown for the night mice (130 trials).

(C) Inset, bottom right: the distributions of the distances the mice were from the maze center in each frame (40-ms): n = 10 mice, 115 trials (day, gold); n = 11 mice, 130 trials (night, blue). The main panel shows the cumulative distributions of the distance from the center for the day (gold) and the night (blue) group.

(D) The same as (C) but shown for the "swap" experiments as explained in Figure 3, where the day group tested at subjective night (green, n = 10 mice, 118 trials) and the night group tested at subjective day (purple, n = 11 mice, 131 trials) have similar performance in the behavioral task as shown in Figure 3B.

(E) Inset, bottom right: the distributions of total time (Δt) that the stimulus projection was within the visual field of mice during the time that they were seeking the stimulus in the center of the maze: day (gold), night (blue). These distributions were obtained by tracking the head position and direction of the mice during swimming trials and assuming a visual field of ±100 degrees [57]: n = 10 mice, 115 trials (day); n = 11 mice, 130 trials (night). The main panel shows the cumulative distributions of Δt for the day (gold) and the night (blue) group.

(F) The same as (E) but shown following the swap, n = 11 mice, 131 trials (night group tested at subjective day, purple); n = 10 mice, 118 trials (day group tested at subjective night, green).

irreversible: once the mice have performed the task at night, they implement the improved strategy also at their subjective day. Finally, we show that the sensitivity of ON-S, OFF-S, and OFF-T alpha RGCs, belonging to the most sensitive RGC types in the mouse retina [46], do not markedly depend on the diurnal rhythm in *ex vivo* retinal preparations. These results have several important consequences related to diurnal effects on retinal computations, behavioral states, and higher-order brain states controlling behavior and sensory processing as discussed below.

Why Is the Detection Threshold of the Most Sensitive RGCs Not under Diurnal Control?

It has been hypothesized previously that many of the diurnal or circadian changes in retinal physiology relate to functional improvements enhancing visual sensitivity at night. Our data now show that the detection thresholds of the most sensitive RGC types in the mouse retina do not have such a diurnal dependency. This is an interesting finding, since previous studies of diurnal changes in retinal responsiveness have relied mainly on ERG response amplitudes, which bear no clear relation to RGC sensitivities at the visual threshold [30–34]. Our results are, to our knowledge, the first direct measurements of diurnal effects on the absolute sensitivity limit of RGCs. One could, of course, always argue that the RGC measurements are done in *ex vivo* preparations, leaving a possibility for *ex vivo* and *in vivo* differences e.g., due to washout of neuromodulators. Furthermore, recent work [58] has provided evidence that RGC signals *in vivo* could depend on the behavioral state of the animal. Such effects requiring potential feedback information from the brain to the retina could, of course, not be detected in *ex vivo* retinal experiments. However, as the behavioral strategy correlates clearly and irreversibly with the diurnal changes in behavioral performance, it is very difficult to explain our main results with any simple neuromodulatory effects in the retina and/or any feedforward-type retinal mechanism. Furthermore, the lowest intensity at which the behavioral psychometric sensitivity function starts to deviate from chance level is very similar between night and day, whereas the slope of the

functions is different. These data are in line with the notion of a shared underlying ultimate constraint from RGCs. Indeed, our recent study on a transgenic mouse line shows that, when ON-S alpha RGC sensitivity is shifted to higher light intensities, the psychometric functions as assessed by the same behavioral photon detection task as here show a similar and robust shift along the intensity axis [46], while their shape remains unaltered. This phenomenon differs significantly from what we see here (Figures 1I and 1J) and supports the idea that the diurnal effects on visual sensitivity observed in this study do not arise in the retina.

Why is there a rich set of physiological changes in the retina that are under diurnal control if these changes do not have any direct impact on retinal computations at the visual threshold? The lack of diurnal control on the output signals of ON-S, OFF-S, and OFF-T alpha RGCs at the sensitivity limit of vision does not exclude the possibility of such effects on retinal computations for other stimuli and light level conditions, neither for these or other RGC types. Indeed, a recent study [40] carried out at stimulus light levels that were ~1,000 times higher than those corresponding to the behavioral threshold intensities in our study and where also directional selectivity occurs, shows circadian modulation of RGC responses across various types *in vivo*. Darkness, however, sets very special functional requirements for vision. The absolute threshold of RGCs and mouse behavior gets very close to the limits posed by physics and retinal noise [46, 59] showing that evolution has optimized this visual computation extremely well. Indeed, it is not clear what biological trade-off might be served here by diurnal effects: maximizing the signal and minimizing noise always seems to be the best thing to do in these conditions, where photons are extremely sparse. Earlier work on primate retina has shown that extremely dim background light causing only a couple of isomerizations during the integration time of the RGC can fundamentally change the noise filtering mechanisms of the inner retina in the ON pathway [54]. Thus, it is likely that the higher scotopic and mesopic light regimes offer a much richer framework for spatiotemporal trade-offs in vision and in retinal computations. At these light levels, computing motion, direction, and orientation provides a rich framework for potential targets for circadian control, whereas, at the visual threshold, such computations are sacrificed for sensitivity [46, 60–62]. In future studies, it will, therefore, be intriguing to seek diurnal effects in well-defined retinal computations and retinal outputs at these higher scotopic and mesopic light levels.

Diurnal Rhythm Can Impact the Behavioral Strategy and the Shape of Psychometric Visual Functions of Mice

Our study is an example of diurnal changes in behavioral strategy on a visually guided performance test. Many past studies assume that animals apply a stable and optimal behavioral strategy and analyze psychometric functions based on these assumptions. Our results underscore the fact that mice are far from "static robots" with a pre-defined set of behavioral rules. Instead, they have a rich set of behavioral strategies to implement, even in the simplest task of photon detection. We show that behavioral strategy itself can be under robust diurnal control, and, once an efficient night-time strategy has been established, it can even be transferred to daytime behavior.

Can we provide a quantitative model for linking the observed changes in behavioral strategy to psychometric functions? It is intriguing that differences in the behavioral strategy as characterized by 12 different features correlated so well with differences in behavioral visual sensitivity as measured in our experiments. However, a more precise understanding of how the shape of the psychometric functions could be predicted from these trackable behavioral features would require more extensive modeling. Our recent study [46] provides a quantitative model for mapping signals originating from sparse photons in a water maze to the ON-S RGC population code and ultimately to psychometric functions through an ideal observer integrating the neural information. However, even if these models account for the differing sampling strategies of visual cues between the day and night group, they fail to predict the entire magnitude of the day-night sensitivity shift. Particularly, the dominant day-night change in the slope of the sensitivity functions observed in this study is hard to implement if one assumes that the downstream circuits integrating neural signals from the retina are in a static state between the day and night groups. Only models linking the downstream readout mechanism with the behavioral state and/or day/night state would allow the observed psychometric functions to be produced. However, constraining the downstream parameters of such models would require data from the neural populations of the mouse brain centers involved in photon detection [63], manipulations of such brain states, e.g., via optogenetic tools, and behavioral sampling by close-loop control of the stimulus, while quantifying the behavior precisely. All of these approaches provide interesting directions for future studies.

What Is the Impact of Higher-Order Brain States on the Diurnal Control of Psychometric Visual Functions?

Our data indirectly point toward changes in the higher-order sensory processing coupled with the observed diurnal changes in behavioral strategy and psychometric functions. In the light of current knowledge, such changes appear plausible: there is an emerging and expanding literature pointing out that the brain's response to sensory inputs is strikingly dependent on the behavioral state, even in awake animals. It has been shown that neural activity patterns, gain stages, gating mechanisms, and sensory processing can vary vastly depending on the behavioral state, e.g., the feeding state [64], thirst [65], locomotion [66–70], fear [71, 72], arousal [73], and attention [74, 75]. Even though the precise neural circuit mechanisms linking behavioral states to brain states are to a large extent unknown [63], some recent work has been able to correlate internal brain states and circuit mechanisms to particular distinct behavioral states, e.g., in reactions to visual threats [72], locomotion [68], or behavioral transitions from active to passive coping [76]. Interestingly, parallel to this literature, other recent studies have shown that many higher-order mechanisms can be under diurnal control: arousal [77], attention [78], mood [79], short- and long-term memory formation [80–84], and the synchrony of cortical activity [85]. We hypothesize that our findings on behavioral search strategies reflect the circadian impact on higher-order brain states and sensory processing. In line with this, and suggestive of a difference in the arousal state between night and day, we observed larger pupil sizes of mice at their subjective night. It has been shown that heightened arousal correlates with larger pupil sizes

[73] and increases the signal-to-noise ratio of visual responses in V1 circuits [86] and enhances contrast detection [87]. The observed difference in pupil size, together with our modeling results, therefore supports the hypothesis that diurnal changes in behavioral repertoire are coupled with diurnal changes in high-order brain states. It would be interesting to rigorously test this hypothesis in future studies.

What Are the Implications of Our Findings for Behavioral Experiments Carried Out on Rodents?

We show that the behavioral performance of mice in a dim-light detection task is robust and stable even across mouse lines when tested at their subjective night. It may be argued that mice, as nocturnal rodents, are also more likely to follow optimal visual strategies and higher-order sensory processing while tested at night. Indeed, our conclusion that higher-order computations also work more effectively at night emphasizes the importance of the nominal night state in behavioral studies of nocturnal rodents. If our findings generalize to other more complex behavioral tasks, it suggests that rodents should be tested at their subjective nighttime. Considering the normal daily rhythm of scientists, this would support the idea of keeping mice in reversed light cycles in their housing conditions by default. It would also be important to study across more behavioral paradigms what conditions produce the highest reproducibility of experimental results.

STAR★METHODS

Detailed methods are provided in the online version of this paper and include the following:

- KEY RESOURCES TABLE
- LEAD CONTACT AND MATERIALS AVAILABILITY
- EXPERIMENTAL MODEL AND SUBJECT DETAILS
  - Mice
- METHOD DETAILS
  - Running wheel experiments
  - Pupil measurements
  - Ganglion cell recordings
  - Behavioral experiments
- QUANTIFICATION AND STATISTICAL ANALYSIS
  - Analysis of RGC features
  - Analysis of behavioral threshold sensitivities
  - Analysis of behavioral search strategy
  - Statistics
- DATA AND CODE AVAILABILITY

SUPPLEMENTAL INFORMATION

Supplemental Information can be found online at https://doi.org/10.1016/j.cub.2019.11.021.

ACKNOWLEDGMENTS

We thank our lab manager, Mr. Sami Minkkinen, and Dr. Daisuke Takeshita in our lab for excellent technical assistance; Drs. Kristian Donner, Robert Lucas, Greg Schwartz, Anna Stöckl, Markku Kilpeläinen, and Johan Westö for valuable comments on the manuscript; Matthew Dunkerley and Sathish Narayanan for the design of the data acquisition software. Support was provided by the Academy of Finland (253314, 256156, 283268, 296269, 305834 to P.A.-L.); the Sigrid Jusélius Foundation (P.A.-L.); the Emil Aaltonen Foundation (P.A.-L.); the Doctoral programme Brain & Mind, University of Helsinki (S.K.); the Oskar Öflund Foundation (S.K.); the Otto A. Malm Foundation (S.K.); the Oskar Öflund Foundation, Finland; and the Ella and Georg Ehrnrooth Foundation (S.K. and T.T.).

AUTHOR CONTRIBUTIONS

S.K. and P.A.-L. designed experiments; S.K. performed RGC and behavioral experiments; T.T. developed the methodology for tracking mice; and S.K., T.T., and P.A.-L. analyzed the data and wrote the manuscript.

DECLARATION OF INTERESTS

Patents related to "A method for performing behavioral experiments with rodents" (T.T. and P.A.-L.): FI patent 2016105 and pending US patent application US15/493,161.

Received: August 31, 2018
Revised: September 1, 2019
Accepted: November 5, 2019
Published: December 19, 2019

REFERENCES

1. Chander, D., and Chichilnisky, E.J. (2001). Adaptation to temporal contrast in primate and salamander retina. J. Neurosci. *21*, 9904–9916.
2. Dowling, J.E. (1967). The site of visual adaptation. Science *155*, 273–279.
3. Dunn, F.A., Lankheet, M.J., and Rieke, F. (2007). Light adaptation in cone vision involves switching between receptor and post-receptor sites. Nature *449*, 603–606.
4. Wark, B., Fairhall, A., and Rieke, F. (2009). Timescales of inference in visual adaptation. Neuron *61*, 750–761.
5. Fain, G.L., Matthews, H.R., Cornwall, M.C., and Koutalos, Y. (2001). Adaptation in vertebrate photoreceptors. Physiol. Rev. *81*, 117–151.
6. Kohn, A. (2007). Visual adaptation: physiology, mechanisms, and functional benefits. J. Neurophysiol. *97*, 3155–3164.
7. Lamb, T.D., and Pugh, E.N.J., Jr. (2004). Dark adaptation and the retinoid cycle of vision. Prog. Retin. Eye Res. *23*, 307–380.
8. Berson, D.M., Dunn, F.A., and Takao, M. (2002). Phototransduction by retinal ganglion cells that set the circadian clock. Science *295*, 1070–1073.
9. Hannibal, J., Hindersson, P., Knudsen, S.M., Georg, B., and Fahrenkrug, J. (2002). The photopigment melanopsin is exclusively present in pituitary adenylate cyclase-activating polypeptide-containing retinal ganglion cells of the retinohypothalamic tract. J. Neurosci. *22*, RC191.
10. Hattar, S., Liao, H.W., Takao, M., Berson, D.M., and Yau, K.W. (2002). Melanopsin-containing retinal ganglion cells: architecture, projections, and intrinsic photosensitivity. Science *295*, 1065–1070.
11. Hattar, S., Lucas, R.J., Mrosovsky, N., Thompson, S., Douglas, R.H., Hankins, M.W., Lem, J., Biel, M., Hofmann, F., Foster, R.G., and Yau, K.W. (2003). Melanopsin and rod-cone photoreceptive systems account for all major accessory visual functions in mice. Nature *424*, 76–81.
12. Lucas, R.J., Douglas, R.H., and Foster, R.G. (2001). Characterization of an ocular photopigment capable of driving pupillary constriction in mice. Nat. Neurosci. *4*, 621–626.
13. Lucas, R.J., Hattar, S., Takao, M., Berson, D.M., Foster, R.G., and Yau, K.W. (2003). Diminished pupillary light reflex at high irradiances in melanopsin-knockout mice. Science *299*, 245–247.
14. Do, M.T., and Yau, K.W. (2010). Intrinsically photosensitive retinal ganglion cells. Physiol. Rev. *90*, 1547–1581.
15. Lucas, R.J., Lall, G.S., Allen, A.E., and Brown, T.M. (2012). How rod, cone, and melanopsin photoreceptors come together to enlighten the mammalian circadian clock. Prog. Brain Res. *199*, 1–18.

16. Doyle, S.E., Grace, M.S., McIvor, W., and Menaker, M. (2002). Circadian rhythms of dopamine in mouse retina: the role of melatonin. Vis. Neurosci. *19*, 593–601.

17. Nir, I., Haque, R., and Iuvone, P.M. (2000). Diurnal metabolism of dopamine in the mouse retina. Brain Res. *870*, 118–125.

18. Tosini, G., and Menaker, M. (1996). Circadian rhythms in cultured mammalian retina. Science *272*, 419–421.

19. Natesan, A.K., and Cassone, V.M. (2002). Melatonin receptor mRNA localization and rhythmicity in the retina of the domestic chick, *Gallus domesticus*. Vis. Neurosci. *19*, 265–274.

20. Chaurasia, S.S., Rollag, M.D., Jiang, G., Hayes, W.P., Haque, R., Natesan, A., Zatz, M., Tosini, G., Liu, C., Korf, H.W., et al. (2005). Molecular cloning, localization and circadian expression of chicken melanopsin (Opn4): differential regulation of expression in pineal and retinal cell types. J. Neurochem. *92*, 158–170.

21. Sakamoto, K., Liu, C., and Tosini, G. (2004). Classical photoreceptors regulate melanopsin mRNA levels in the rat retina. J. Neurosci. *24*, 9693–9697.

22. Sakamoto, K., Liu, C., Kasamatsu, M., Pozdeyev, N.V., Iuvone, P.M., and Tosini, G. (2005). Dopamine regulates melanopsin mRNA expression in intrinsically photosensitive retinal ganglion cells. Eur. J. Neurosci. *22*, 3129–3136.

23. Fukuhara, C., Liu, C., Ivanova, T.N., Chan, G.C., Storm, D.R., Iuvone, P.M., and Tosini, G. (2004). Gating of the cAMP signaling cascade and melatonin synthesis by the circadian clock in mammalian retina. J. Neurosci. *24*, 1803–1811.

24. Ivanova, T.N., and Iuvone, P.M. (2003). Circadian rhythm and photic control of cAMP level in chick retinal cell cultures: a mechanism for coupling the circadian oscillator to the melatonin-synthesizing enzyme, arylalkylamine N-acetyltransferase, in photoreceptor cells. Brain Res. *991*, 96–103.

25. Astakhova, L.A., Nikolaeva, D.A., Fedotkina, T.V., Govardovskii, V.I., and Firsov, M.L. (2017). Elevated cAMP improves signal-to-noise ratio in amphibian rod photoreceptors. J. Gen. Physiol. *149*, 689–701.

26. Dalal, J.S., Jinks, R.N., Cacciatore, C., Greenberg, R.M., and Battelle, B.A. (2003). Limulus opsins: diurnal regulation of expression. Vis. Neurosci. *20*, 523–534.

27. Pierce, M.E., Sheshberadaran, H., Zhang, Z., Fox, L.E., Applebury, M.L., and Takahashi, J.S. (1993). Circadian regulation of iodopsin gene expression in embryonic photoreceptors in retinal cell culture. Neuron *10*, 579–584.

28. LaVail, M.M. (1976). Rod outer segment disk shedding in rat retina: relationship to cyclic lighting. Science *194*, 1071–1074.

29. Xue, Y., Shen, S.Q., Corbo, J.C., and Kefalov, V.J. (2015). Circadian and light-driven regulation of rod dark adaptation. Sci. Rep. *5*, 17616.

30. Baba, K., Pozdeyev, N., Mazzoni, F., Contreras-Alcantara, S., Liu, C., Kasamatsu, M., Martinez-Merlos, T., Strettoi, E., Iuvone, P.M., and Tosini, G. (2009). Melatonin modulates visual function and cell viability in the mouse retina via the MT1 melatonin receptor. Proc. Natl. Acad. Sci. USA *106*, 15043–15048.

31. Barnard, A.R., Hattar, S., Hankins, M.W., and Lucas, R.J. (2006). Melanopsin regulates visual processing in the mouse retina. Curr. Biol. *16*, 389–395.

32. Cameron, M.A., Barnard, A.R., Hut, R.A., Bonnefont, X., van der Horst, G.T., Hankins, M.W., and Lucas, R.J. (2008). Electroretinography of wild-type and Cry mutant mice reveals circadian tuning of photopic and mesopic retinal responses. J. Biol. Rhythms *23*, 489–501.

33. Cameron, M.A., and Lucas, R.J. (2009). Influence of the rod photoresponse on light adaptation and circadian rhythmicity in the cone ERG. Mol. Vis. *15*, 2209–2216.

34. Lavoie, J., Gagné, A.M., Lavoie, M.P., Sasseville, A., Charron, M.C., and Hébert, M. (2010). Circadian variation in the electroretinogram and the presence of central melatonin. Doc. Ophthalmol. *120*, 265–272.

35. Ribelayga, C., Cao, Y., and Mangel, S.C. (2008). The circadian clock in the retina controls rod-cone coupling. Neuron *59*, 790–801.

36. Jin, N.G., Chuang, A.Z., Masson, P.J., and Ribelayga, C.P. (2015). Rod electrical coupling is controlled by a circadian clock and dopamine in mouse retina. J. Physiol. *593*, 1597–1631.

37. Bloomfield, S.A., and Völgyi, B. (2004). Function and plasticity of homologous coupling between AII amacrine cells. Vision Res. *44*, 3297–3306.

38. Hu, E.H., Pan, F., Völgyi, B., and Bloomfield, S.A. (2010). Light increases the gap junctional coupling of retinal ganglion cells. J. Physiol. *588*, 4145–4163.

39. Pack, W., Hill, D.D., and Wong, K.Y. (2015). Melatonin modulates M4-type ganglion-cell photoreceptors. Neuroscience *303*, 178–188.

40. Hong, G., Fu, T.M., Qiao, M., Viveros, R.D., Yang, X., Zhou, T., Lee, J.M., Park, H.G., Sanes, J.R., and Lieber, C.M. (2018). A method for single-neuron chronic recording from the retina in awake mice. Science *360*, 1447–1451.

41. Zhao, W.J., Zhang, M., Miao, Y., Yang, X.L., and Wang, Z. (2010). Melatonin potentiates glycine currents through a PLC/PKC signalling pathway in rat retinal ganglion cells. J. Physiol. *588*, 2605–2619.

42. Bassi, C.J., and Powers, M.K. (1986). Daily fluctuations in the detectability of dim lights by humans. Physiol. Behav. *38*, 871–877.

43. O'Keefe, L.P., and Baker, H.D. (1987). Diurnal changes in human psychophysical luminance sensitivity. Physiol. Behav. *41*, 193–200.

44. Balkema, G.W., Cusick, K., and Nguyen, T.H. (2001). Diurnal variation in synaptic ribbon length and visual threshold. Vis. Neurosci. *18*, 789–797.

45. Astakhova, L.A., Samoiliuk, E.V., Govardovskii, V.I., and Firsov, M.L. (2012). cAMP controls rod photoreceptor sensitivity via multiple targets in the phototransduction cascade. J. Gen. Physiol. *140*, 421–433.

46. Smeds, L., Takeshita, D., Turunen, T., Tiihonen, J., Westö, J., Martyniuk, N., Seppänen, A., and Ala-Laurila, P. (2019). Paradoxical rules of spike train decoding revealed at the sensitivity limit of vision. Neuron *104*, 576–587.e11.

47. Goto, M., Oshima, I., Tomita, T., and Ebihara, S. (1989). Melatonin content of the pineal gland in different mouse strains. J. Pineal Res. *7*, 195–204.

48. Roseboom, P.H., Namboodiri, M.A., Zimonjic, D.B., Popescu, N.C., Rodriguez, I.R., Gastel, J.A., and Klein, D.C. (1998). Natural melatonin 'knockdown' in C57BL/6J mice: rare mechanism truncates serotonin N-acetyltransferase. Brain Res. Mol. Brain Res. *63*, 189–197.

49. Nakahara, D., Nakamura, M., Iigo, M., and Okamura, H. (2003). Bimodal circadian secretion of melatonin from the pineal gland in a living CBA mouse. Proc. Natl. Acad. Sci. USA *100*, 9584–9589.

50. Baden, T., Berens, P., Franke, K., Román Rosón, M., Bethge, M., and Euler, T. (2016). The functional diversity of retinal ganglion cells in the mouse. Nature *529*, 345–350.

51. Bae, J.A., Mu, S., Kim, J.S., Turner, N.L., Tartavull, I., Kemnitz, N., Jordan, C.S., Norton, A.D., Silversmith, W.M., Prentki, R., et al.; Eyewirers (2018). Digital museum of retinal ganglion cells with dense anatomy and physiology. Cell *173*, 1293–1306.

52. Rheaume, B.A., Jereen, A., Bolisetty, M., Sajid, M.S., Yang, Y., Renna, K., Sun, L., Robson, P., and Trakhtenberg, E.F. (2018). Single cell transcriptome profiling of retinal ganglion cells identifies cellular subtypes. Nat. Commun. *9*, 2759.

53. Dunn, F.A., and Rieke, F. (2008). Single-photon absorptions evoke synaptic depression in the retina to extend the operational range of rod vision. Neuron *57*, 894–904.

54. Ala-Laurila, P., and Rieke, F. (2014). Coincidence detection of single-photon responses in the inner retina at the sensitivity limit of vision. Curr. Biol. *24*, 2888–2898.

55. Takeshita, D., Smeds, L., and Ala-Laurila, P. (2017). Processing of single-photon responses in the mammalian On and Off retinal pathways at the sensitivity limit of vision. Philos. Trans. R. Soc. Lond. B Biol. Sci. *372*. Published online April 5, 2017. https://doi.org/10.1098/rstb.2016.0073.

56. Spink, A.J., Tegelenbosch, R.A., Buma, M.O., and Noldus, L.P. (2001). The EthoVision video tracking system–a tool for behavioral phenotyping of transgenic mice. Physiol. Behav. *73*, 731–744.

57. Dräger, U.C. (1975). Receptive fields of single cells and topography in mouse visual cortex. J. Comp. Neurol. *160*, 269–290.

58. Schröder, S., Steinmetz, N.A., Krumin, M., Pachitariu, M., Rizzi, M., Lagnado, L., Harris, K.D., and Carandini, M. (2019). Retinal outputs depend on behavioural state. bioRxiv. https://doi.org/10.1101/638049v1.

59. Naarendorp, F., Esdaille, T.M., Banden, S.M., Andrews-Labenski, J., Gross, O.P., and Pugh, E.N.J., Jr. (2010). Dark light, rod saturation, and the absolute and incremental sensitivity of mouse cone vision. J. Neurosci. *30*, 12495–12507.

60. Grimes, W.N., Schwartz, G.W., and Rieke, F. (2014). The synaptic and circuit mechanisms underlying a change in spatial encoding in the retina. Neuron *82*, 460–473.

61. Kuo, S.P., Schwartz, G.W., and Rieke, F. (2016). Nonlinear spatiotemporal integration by electrical and chemical synapses in the retina. Neuron *90*, 320–332.

62. Yao, X., and Field, G.D. (2019). Inhibition controls receptive field size, sensitivity, and response polarity of direction selective ganglion cells near the threshold of vision. bioRxiv. https://doi.org/10.1101/683961.

63. Stringer, C., Pachitariu, M., Steinmetz, N., Reddy, C.B., Carandini, M., and Harris, K.D. (2019). Spontaneous behaviors drive multidimensional, brainwide activity. Science *364*, 255.

64. Filosa, A., Barker, A.J., Dal Maschio, M., and Baier, H. (2016). Feeding state modulates behavioral choice and processing of prey stimuli in the zebrafish tectum. Neuron *90*, 596–608.

65. Allen, W.E., Chen, M.Z., Pichamoorthy, N., Tien, R.H., Pachitariu, M., Luo, L., and Deisseroth, K. (2019). Thirst regulates motivated behavior through modulation of brainwide neural population dynamics. Science *364*, 253.

66. Bennett, C., Arroyo, S., and Hestrin, S. (2013). Subthreshold mechanisms underlying state-dependent modulation of visual responses. Neuron *80*, 350–357.

67. Fu, Y., Tucciarone, J.M., Espinosa, J.S., Sheng, N., Darcy, D.P., Nicoll, R.A., Huang, Z.J., and Stryker, M.P. (2014). A cortical circuit for gain control by behavioral state. Cell *156*, 1139–1152.

68. Lee, A.M., Hoy, J.L., Bonci, A., Wilbrecht, L., Stryker, M.P., and Niell, C.M. (2014). Identification of a brainstem circuit regulating visual cortical state in parallel with locomotion. Neuron *83*, 455–466.

69. Maimon, G., Straw, A.D., and Dickinson, M.H. (2010). Active flight increases the gain of visual motion processing in *Drosophila*. Nat. Neurosci. *13*, 393–399.

70. Niell, C.M., and Stryker, M.P. (2010). Modulation of visual responses by behavioral state in mouse visual cortex. Neuron *65*, 472–479.

71. Herry, C., Ciocchi, S., Senn, V., Demmou, L., Müller, C., and Lüthi, A. (2008). Switching on and off fear by distinct neuronal circuits. Nature *454*, 600–606.

72. Salay, L.D., Ishiko, N., and Huberman, A.D. (2018). A midline thalamic circuit determines reactions to visual threat. Nature *557*, 183–189.

73. McGinley, M.J., David, S.V., and McCormick, D.A. (2015). Cortical membrane potential signature of optimal states for sensory signal detection. Neuron *87*, 179–192.

74. Maimon, G. (2011). Modulation of visual physiology by behavioral state in monkeys, mice, and flies. Curr. Opin. Neurobiol. *21*, 559–564.

75. Wimmer, R.D., Schmitt, L.I., Davidson, T.J., Nakajima, M., Deisseroth, K., and Halassa, M.M. (2015). Thalamic control of sensory selection in divided attention. Nature *526*, 705–709.

76. Andalman, A.S., Burns, V.M., Lovett-Barron, M., Broxton, M., Poole, B., Yang, S.J., Grosenick, L., Lerner, T.N., Chen, R., Benster, T., et al. (2019). Neuronal dynamics regulating brain and behavioral state transitions. Cell *177*, 970–985.

77. Aston-Jones, G., Chen, S., Zhu, Y., and Oshinsky, M.L. (2001). A neural circuit for circadian regulation of arousal. Nat. Neurosci. *4*, 732–738.

78. Valdez, P., Ramírez, C., García, A., Talamantes, J., Armijo, P., and Borrani, J. (2005). Circadian rhythms in components of attention. Biol. Rhythm Res. *36*, 57–65.

79. Fernandez, D.C., Fogerson, P.M., Lazzerini Ospri, L., Thomsen, M.B., Layne, R.M., Severin, D., Zhan, J., Singer, J.H., Kirkwood, A., Zhao, H., et al. (2018). Light affects mood and learning through distinct retina-brain pathways. Cell *175*, 71–84.

80. Gerstner, J.R., Lyons, L.C., Wright, K.P., Jr., Loh, D.H., Rawashdeh, O., Eckel-Mahan, K.L., and Roman, G.W. (2009). Cycling behavior and memory formation. J. Neurosci. *29*, 12824–12830.

81. Kondratova, A.A., Dubrovsky, Y.V., Antoch, M.P., and Kondratov, R.V. (2010). Circadian clock proteins control adaptation to novel environment and memory formation. Aging (Albany N.Y.) *2*, 285–297.

82. Lyons, L.C., and Roman, G. (2008). Circadian modulation of short-term memory in *Drosophila*. Learn. Mem. *16*, 19–27.

83. Ruby, N.F., Hwang, C.E., Wessells, C., Fernandez, F., Zhang, P., Sapolsky, R., and Heller, H.C. (2008). Hippocampal-dependent learning requires a functional circadian system. Proc. Natl. Acad. Sci. USA *105*, 15593–15598.

84. Van der Zee, E.A., Havekes, R., Barf, R.P., Hut, R.A., Nijholt, I.M., Jacobs, E.H., and Gerkema, M.P. (2008). Circadian time-place learning in mice depends on Cry genes. Curr. Biol. *18*, 844–848.

85. Beaman, C.B., Eagleman, S.L., and Dragoi, V. (2017). Sensory coding accuracy and perceptual performance are improved during the desynchronized cortical state. Nat. Commun. *8*, 1308.

86. Vinck, M., Batista-Brito, R., Knoblich, U., and Cardin, J.A. (2015). Arousal and locomotion make distinct contributions to cortical activity patterns and visual encoding. Neuron *86*, 740–754.

87. Kim, D., Lokey, S., and Ling, S. (2017). Elevated arousal levels enhance contrast perception. J. Vis. *17*, 14.

88. Efron, B., and Tibshirani, R. (1993). An Introduction to the Bootstrap (Chapman & Hall).

89. Butler, M.P., and Silver, R. (2011). Divergent photic thresholds in the non-image-forming visual system: entrainment, masking and pupillary light reflex. Proc. Biol. Sci. *278*, 745–750.

90. Govardovskii, V.I., Fyhrquist, N., Reuter, T., Kuzmin, D.G., and Donner, K. (2000). In search of the visual pigment template. Vis. Neurosci. *17*, 509–528.

91. Toda, K., Bush, R.A., Humphries, P., and Sieving, P.A. (1999). The electroretinogram of the rhodopsin knockout mouse. Vis. Neurosci. *16*, 391–398.

92. Hecht, S., Haig, C., and Chase, A.M. (1937). The influence of light adaptation on subsequent dark adaptation of the eye. J. Gen. Physiol. *20*, 831–850.

93. Lee, K.A., Nawrot, M., Garwin, G.G., Saari, J.C., and Hurley, J.B. (2010). Relationships among visual cycle retinoids, rhodopsin phosphorylation, and phototransduction in mouse eyes during light and dark adaptation. Biochemistry *49*, 2454–2463.

STAR★METHODS

KEY RESOURCES TABLE

REAGENT or RESOURCE	SOURCE	IDENTIFIER
Chemicals, Peptides, and Recombinant Proteins		
Ames' Medium	Sigma-Aldrich	Cat# A1420
HiLyte Fluor 750 hydrazide	AnaSpec	Cat# AS-81268
Experimental Models: Organisms/Strains		
C57BL/6J	Charles River	RRID:IMSR_JAX:000664
CBA/CaJ	The Jackson Laboratory	RRID:IMSR_JAX:000654
Software and Algorithms		
MATLAB (version: R2014b and onward)	The Mathworks	https://se.mathworks.com/products/matlab.html
OriginPro (version: 2018b)	OriginLab	http://www.originlab.com
IBM SPSS (version: 22)	IBM SPSS Statistics	https://www.ibm.com/products/spss-statistics
Symphony (version: 1.2.1.0 and onward)	Symphony-DAS; Ala-Laurila Lab	https://github.com/Symphony-DAS/symphony-v1; https://github.com/ala-laurila-lab/Symphony-1.x
Andor iQ3	Oxford Instruments	https://andor.oxinst.com/products/iq-live-cell-imaging-software/andor-iq3
ImageJ (version: 1.47)	NIH	https://imagej.nih.gov/ij
Python (version: 3.6)	Python Software Foundation	https://www.python.org
OpenCV (version: 3.4)	OpenCV team	https://opencv.org
NumPy (version: 1.16)	NumPy developers	http://www.numpy.org
SciPy (version: 1.2)	SciPy developers	https://www.scipy.org
PySide2 (version: 5.6)	Qt Project	https://wiki.qt.io/PySide
TensorFlow (version: 1.12 GPU)	Google Brain Team	https://www.tensorflow.org
VirtualDub (version: 1.10.4)	virtualdub.org	http://virtualdub.org
Java (version: SE 7)	Oracle	https://www.oracle.com
Micro-Manager (version 1.4.22)	Open Imaging	https://micro-manager.org
Stan platform	The Stan Development Team	http://mc-stan.org
Multi-Device Interface Software for running wheel recording	Columbus Instruments	http://www.colinst.com/products/multi-device-interface-mdi-software
BioRender	BioRender	biorender.com
Other		
8 Station Home Cage Running Wheel System with Software	Columbus Instruments	0297-8
Microscope for ganglion cell recordings	Nikon	Eclipse FN1
Amplifier for ganglion cell recordings	Axon Instruments / Molecular Devices	MultiClamp 700B
Excitation light source for epifluorescence	Excelitas Technologies	X-Cite 120Q
Camera for fluorescence imaging	Andor technology, Oxford Instruments	iXon Ultra 897 EMCCD
Camera for tracking mouse behavior and measuring pupil size	Watec	Wat-902H2 Ultimate
Optometer for light calibrations	UDT Instruments	S470 & S450 with 268R sensor
Spectrometer for spectral irradiance measurements of light stimuli	Ocean Optics	JAZ-COMBO

LEAD CONTACT AND MATERIALS AVAILABILITY

Further information and requests for resources and reagents should be directed to and will be fulfilled by the Lead Contact, Petri Ala-Laurila (Petri.ala-laurila@helsinki.fi). This study did not generate new unique reagents.

EXPERIMENTAL MODEL AND SUBJECT DETAILS

Mice

Melatonin deficient mice (C57BL/6J; Charles River Laboratories, Sulzfeld, Germany; RRID:IMSR_JAX:000654) and melatonin proficient mice (CBA/CaJ; Jackson Laboratory, Bar Harbor, ME, USA; RRID:IMSR_JAX:000664) were used in all experiments (males and females at the age of 8-40 weeks). Mice were housed in two rooms with different 12 h/12h light/dark cycles: lights were on from 06:00 to 18:00 in the room designed for the ''day group'' (C57: 6 females and 5 males; CBA: 5 females and 5 males) and from 20:00 to 08:00 in the room designed for the ''night group'' (C57: 5 females and 5 males; CBA: 5 females and 5 males, CBA ZT21 night group: 3 females and 6 males; see Figure 1B). Animals were acclimated to their light cycles for at least 20 days before the experiments. The lighting of both rooms was monitored with a data-logging lux meter (model HHLM112SD, Omega Engineering Inc). The light intensity during the ''day'' time was in the range 100-700 lux (depending mainly on the cage location in the rooms) and always well beyond the threshold light level needed for photoentrainment of mice for diurnal rhythms [89]. All animal procedures were performed according to the protocols approved by the Regional State Administration Agency of for Southern Finland. Sample sizes were not determined prior to the experiments, and the investigators were not blinded to the mouse strains.

METHOD DETAILS

Running wheel experiments

The running wheel activity of mice was recorded from single-housed male mice in cages (26.7 × 20.7 × 14 cm) equipped with running wheels (9.5 cm in diameter; Columbus Instruments International). The data was acquired in each case consecutively for 20 days using 10-min time bins with the software provided by Columbus Instruments (Multi-Device Interface Software) and further analyzed in MATLAB (R2014b).

Pupil measurements

The pupil areas of dark-adapted mice were measured as previously described [46] to allow us to estimate the light intensities used in behavioral experiments in the rates of photoisomerizations in rods (R*/rod/s, see below). Briefly, these measurements were done in darkness in a dry water maze during the same time interval as the behavioral experiments were performed. The mouse was held from its tail at the center of the maze and monitored with an IR-sensitive camera (WAT-902H2, Watec) with a macro lens (MLH-10X macro zoom lens, Computar) at a distance of ~20 cm from the mouse's head. The IR LEDs of the experimental setup were turned on to allow the mouse pupils to be visualized. Pupil areas were measured from single frames of the videos using ImageJ by tracking the border of the pupil in each frame (1.47v, National Institute of Health, USA).

Ganglion cell recordings

Ex vivo retinal preparations were harvested from C57 and CBA mice in closely matching diurnal times with the behavioral experiments considering the previous estimates of the melatonin cycle in CBA mice [49]. The dissection time for the ''day'' experiments was 3 hours after light onset (ZT3) and for the ''night'' experiments 7.5 hours from light offset (ZT19.5). The recordings were done between ZT3–ZT8 (day experiments) and ZT20–ZT23 (night experiments).

Ganglion cell recordings followed previously described procedures [46, 54]. Briefly, the mice were dark-adapted for a minimum of 2 hours and sacrificed by rapid cervical dislocation. Their eyes were enucleated, hemisected, the vitreous was removed, and the eyecups were stored in a light-tight container at 32°C in oxygenated (95% O_2/5% CO_2) Ames solution (Sigma, A-1420; osmolality adjusted to 280 ± 2 mOsm/kg). All procedures were done under infrared illumination (> 900 nm) using night vision goggles (PVS-7-1600, B.E. Meyers) and IR pocket scopes (D7200-I-1600, B.E. Meyers) attached to the dissection microscope. Pieces of the retina were gently isolated from the pigment epithelium and placed on a poly-D-lysine coverslip (BioCoat, Corning, Discovery Labware, Inc.) photoreceptor side down. The retina was then transferred to the recording chamber and perfused with warm (32 ± 1°C) Ames solution at a flow rate of 8 ml/min. The preparations were visualized using IR light (940 nm; turned off during recordings) and a CCD camera (Wat-902HS, Watec) attached to the microscope.

All experiments were performed in flat-mount preparations of the retina. ON sustained, OFF sustained, and OFF transient alpha ganglion cells (ON-S, OFF-S and OFF-T) were identified based on their large soma size and their typical light responses as previously described [46]. In a subset of experiments, the dendritic morphology of cells was verified by filling the cells with a fluorescent dye (HiLyte Fluor 750 hydrazide, AnaSpec, AS-81268) and imaging the cells (Andor iXon Ultra 897 EMCCD) following fluorescence excitation (peak at 740 nm; width 35nm, X-Cite 120Q, Excelitas Technologies). The cell morphology was confirmed to be consistent with ON-S, OFF-S, or OFF-T alpha RGCs. We recorded the light-evoked action potentials in cell-attached patch clamp configuration.

Calibrated spatially uniform flashes (20-ms in duration, circular spot, ~580 μm in diameter) centered on the target cell were used in RGC recordings from a blue LED (peak at 470 nm). Stimulus intensities were set by neutral density filters and by controlling the current driving the LEDs. Light intensities were calibrated with an optometer (S450 with the sensor 268R, UDT Instruments) and the spectrum was measured with a spectrometer (Jaz spectrometer, OceanOptics). Calibrated photon fluxes were converted to photoisomerizations per rod per second (R*/rod/s) based on rhodopsin absorption spectrum [90] with the wavelength of peak sensitivity for the mouse rhodopsin, λ_{max} = 497 nm [91], the measured LED spectrum and the peak rod collecting area of 0.6 μm^2 (see [46], STAR Methods for a detailed description of the peak collecting area estimation).

Behavioral experiments

The visual threshold of mice was determined as previously described [46]. Shortly, behavioral experiments carried out in a black six-armed water maze in darkness monitored the ability of dark-adapted mice to find a dim light spot. The mice were placed in the center of the maze in a transparent tube and allowed to orient for ~5 s. Then the transparent tube was removed, allowing the mice to approach the stimulus light located in one of the six arms. The choice was defined as correct if the mouse entered the stimulus corridor before entering any other corridor. All experiments were done in darkness using night-vision goggles. The body and head positions of the mouse were monitored during the behavioral trials under IR illumination using a sensitive CCD camera (WAT-902H2 ultimate, Watec; equipped with a 12VM412ASIR lens, Tamron) and our fully-automated system for tracking mouse behavior [46]. All experiments were recorded using an open-source video capture software (VirtualDub 1.10.4, http://virtualdub.org) and stored on the computer in the AVI format.

The mice were first trained in dim ambient illumination to associate the stimulus light with an escape ramp from the water (~20°C) using easily detectable stimulus light intensity (~200 000 R*/rod/s) (Figure 1A). After the training, the mice learned to make the correct choice in $\geq$ 80% of the trials (Figures 1F and 1H). This took 12 days for C57 mice and 10 days for CBA mice and was always performed during the subjective day. Thereafter, the mice (21 C57 and 20 CBA divided into the day and the night groups) were tested with a sequence of intensities (200 000 – 0.001 R*/rod/s, one intensity per day, 4 trials per mouse per day), starting at the highest intensity, the intensity was subsequently decreased each day until the mice made a choice completely randomly. The location of the stimulus light was randomized across trials. At the end of the experimental series, the mice were re-tested with a high stimulus intensity to make sure that no significant changes had happened in their overall ability to perform the task (i.e., that the fraction of correct choices $\geq$ 80% of the trials at this high intensity).

The stimuli consisted of a circular plexi-diffusor window (~40 mm in diameter) located at the end of each corridor. The stimulus window was continuously illuminated by a green LED (peak at 515 nm) and narrow-band filtered with a 512-nm interference filter (~10-nm transmission bandwidth) during each experimental trial. The light intensity was set by neutral density filters and by controlling the current driving the LEDs. Light intensities were calibrated with an optometer (Models S470 & S450 with 268R sensor, UDT Instruments) at the level of the mouse cornea at the center of the maze. The spectral irradiances of stimuli were measured with a spectrometer (Jaz spectrometer, Ocean Optics) The photoisomerization rates were calculated based on the projected size of the stimulus spot on the retina while taking into account the pupil size of mice [46].

The timing of the measurements was defined as three hours from light onset (ZT3) for the day group and three hours from light offset (ZT15) for the night group. We also tested CBA-mice at their supposed melatonin peak at night, ZT21 [49]. The mice were always dark adapted for a minimum of 2 hours before the experiments. We have confirmed by comparing RGC sensitivities obtained after 2 hours versus overnight in our laboratory that the 2-hour dark adaptation time is sufficient for reaching a fully dark-adapted RGC state. Furthermore, previous literature both at the level of *in vivo* retinal samples in mice as well as human psychophysical experiments confirm that dark-adaptation is complete within 2 hours [92, 93].

We verified that the lighting conditions of the behavioral experiments did not affect the diurnal activity rhythm. First, we measured whether the dark adaptation and the testing period in darkness could alter the running wheel activity of the day-group (Figure S1A). The mice were given a three-hour dark period after 1 hour after light onset (ZT1), mimicking the testing conditions of the day-group (1 hour of light exposure followed by 2 hours of dark adaptation and 1 hour of testing in the dark). We did not find any shift in the activity rhythms measured during the dark pulse compared to the activity without the dark pulse. Second, we checked that the light intensities corresponding to the light stimuli used in the water maze experiments during the dark period did not affect the running wheel activity of the night group (Figure S1B). We showed the mice four 5 s flashes corresponding to the median swimming time of mice during the water maze experiments. These flashes were delivered at the subjective testing time of the night group (3 hours from light offset, ZT3). The stimulus was matched to the water maze experimental conditions and the intensities decreased daily by a factor of 10 as in the behavioral experiments. We did not find any shift in the activity rhythms.

QUANTIFICATION AND STATISTICAL ANALYSIS

Analysis of RGC features

Two-alternative forced choice (2AFC) ideal observer analysis was performed to define the sensitivity limit of RGCs [54]. Briefly, a correlation of the pre- and post-flash firing rates was compared with an average flash response (discriminant). The average flash response was computed across all other epochs except for the one under examination. The choice was assigned based on the higher correlation value. We defined the intensity giving rise to 75% correct choices in the task as the sensitivity threshold for RGCs. The means presented in Figure 2J and in Table S1 are geometric means. A time window of 450 ms preceding and following the 20 ms flash was used in all of the analyses.

To calculate the RGC integration time and flash sensitivity (see below) we used baseline-corrected peristimulus-time-histograms (PSTHs) for ON-S and OFF-S RGCs. However, for OFF-T RGCs with a biphasic response, we instead used the absolute values of the PSTHs. The integration time was obtained as the integral of the normalized PSTH (normalized to the transient peak for OFF-T RGCs). Flash sensitivity, in turn, was estimated as the response per absorbed photon by dividing the average response (spike count difference: response versus baseline firing) with the flash strength (intensity in R*). The response slopes were calculated in a similar fashion.

For ON-S and OFF-S RGCs, the response was defined as the average spike count difference (between post-flash and pre-flash firing rates) whereas for the OFF-T RGCs it was defined as the absolute spike count difference (between baseline subtracted post-flash and pre-flash firing rates).

The normality of the parameter distributions was tested with Kolmogorov-Smirnov normality test. The features that were not normally distributed were tested with Mann Whitney U -test and the rest with two-independent samples t test.

Analysis of behavioral threshold sensitivities

The metric for behaviorally measured visual sensitivity was defined as the percentage of trials when the mice found the right corridor (entered the stimulus corridor as the first choice) as a function of stimulus light intensity (see Figures 1I and 1J) [46]. A modified Hill function was fitted to the behavioral response-intensity curves:

$$F = 0.17 + F_{max}\frac{I^n}{I^n + K_m^n}, \quad (1)$$

where F is the fraction of correct choices at intensity I, F_{max} the maximal fraction of correct choices, K_m the intensity corresponding to half-maximal F and n the slope of the curve. The factor 0.17 ($\approx$1/6) represents chance level (i.e., behavioral performance converges to the chance level at the lowest light levels). The fits were weighted with $1/SEM^2$. We calculated the posterior probabilities for the Hill function parameters using logistic regression to show that the slope parameter n was larger for the night group than for the day group ($p < 0.01$) and the half-saturating intensity parameter K_m was larger for the day group as compared to the night group ($p < 0.03$).The logistic regression fit was calculated using Stan platform (http://mc-stan.org/) with 200 000 samples taken to estimate the parameters.

Analysis of behavioral search strategy

To estimate the behavioral strategy of mice, we obtained the head- and body-position as well as the head-direction of the mouse in each frame from our automated video-tracking software. We analyzed the body-position and head-direction on the series of frames constituting the mouse swimming path to derive a set of quantitative features of the animal's behavior (see below). To exclude the time when the mouse had detected the stimulus and merely swam toward it, we focused on the early part of each trial where the mouse was at the center of the maze looking for the stimulus (central area corresponding to 50% of the maze area excluding corridors). In this constrained area, a decision was defined to be made when a mouse exited the center region toward any corridor. The analysis was done on the intensity range corresponding to the greatest day–night difference in the fraction of correct choices for the C57 mice: 0.03–0.14 R*/rod/s. In all of the analyses, we assumed ± 100° field of view centered at the mouse nose. This is a conservative assumption based on [57], where the mouse binocular visual field was estimated to be at least 120° (±60°). We checked the robustness of the analysis with fields of view of ± 15°, ± 60°, ± 100° and ± 120°. The main conclusions held across all tested visual fields.

The features included in the analysis were the following (see also Table 1): *swimming distance* (= the length of the swimming path during a trial, mm); *swimming distance from center* (= median distance of the mouse from the maze center during its swimming path, mm); *swimming speed* (= median swimming speed of the mouse, mm/s); *swimming time* (= total swimming time inside the central region, s); *angular velocity* (= median turning speed of the mouse during its swimming path, degrees/s); *heading angle* (= median angle between the head-direction and the direction of the stimulus, degrees); *meander* or "*zigzag*" (= the change in direction of head movement relative to swimming distance, degrees/mm); *number of corridors seen* (= how many of the six LEDs that have been inside the visual field of the mouse during its swimming path); *time stimulus in view* (= the accumulated time that the stimulus stayed within the visual field, s); *times correct corridor comes into view* (= the number of times that the stimulus enters the visual field. The number increases every time the mouse looks at the stimulus); *times new corridor comes into view* (= the number of times that any LED, including the stimulus LED, was within the visual field. The number increases every time when the mouse looks at the same LED again after having looked at another LED); *turn angle* (= the cumulative change in head direction during the swimming path, degrees. A large turn angle indicates circling movements.

Statistics

All data analysis and result figures were done in MATLAB (version R2014B and onward), Origin (OriginPro 2018) or SPSS (version 22.0.0.1). All data are presented as mean ± standard error of mean (SEM) unless otherwise stated in figure legends. Details of the sample size (n) for each experiment can be found in the figure legends. Statistical significance was tested with two-independent-samples t test and Mann-Whitney U test for those features that were not normally distributed. Paired samples t test was used to compare the difference in pupil size between day and night. Nonparametric Mann Whitney U test was used to test the difference in medians between night and day in all of the continuous behavioral features that we obtained from the video-tracked data. For the discretized behavioral features, we used a two-tailed permutation test with the mean as a test statistic. A p value of 0.05 was used to define significance in all test. All tests used for p values were two-tailed. The SEMs were calculated per light intensity from the means of individual mouse performances.

DATA AND CODE AVAILABILITY

The datasets and code generated during the current study are available from the corresponding author on request.